Journal of Engineering Mathematics **40:** 1–16, 2001.

Evaluation of the Green function for 3-D wave-body interactions in a channel*

JINZHU XIA
Centre for Oil and Gas Engineering, The University of Western Australia, Nedlands, WA6907, Australia, (e-mail: jinzhu.xia@uwa.edu.au)

Recieved 2 April 1998; accepted in revised form 17 July 2000

Abstract. This study deals with a 3-D boundary-value problem that arises when free-surface waves interact with a stationary body or body system in a channel or wave tank of rectangular cross-section. A consistent asymptotic analysis and an efficient numerical solution is presented of the Green function that satisfies the linear free- surface condition and the non-penetration condition on the channel bottom and the sidewalls. The formulation is based on the open-sea Green function and the complete series of images is evaluated accurately based on the asymptotic analysis. It is demonstrated that the Green function has a square-root singular behavior due to the sidewalls when the wave frequency approaches one of the resonant frequencies. The numerical results for the Green function presented in this paper are believed to have an absolute accuracy of 10^{-5}.

Key words: Green function, wave hydrodynamics, tank resonance, asymptotic analysis, channel interference.

1. Introduction

Hydrodynamics of a body or body system in a channel is of significant importance in two obvious engineering applications. First, in a river (water channel) or harbor transportation system, wave interference effects between bodies and boundaries play an important role. Secondly, model experiments of hydrodynamic forces and the resulting responses of offshore structures such as semi-submersibles and tension leg platforms are often carried out in towing tanks with parallel sidewalls; when evaluating the behavior of structures in the sea based on the results of model tests in towing tanks, it is important to account for the interference effects due to wave reflections from the tank walls.

Potential theory is often used to describe hydrodynamic wave-body interaction problems. If we consider the fluid to be an incompressible inviscid fluid with a free surface, the resulting problem involves the solution of Laplace's equation subject to various body, boundary and free-surface conditions. For arbitrary-shaped bodies, the boundary-element method is a powerful numerical method for solving these equations. If a Green function is constructed to satisfy the conditions over all boundary surfaces of the fluid domain except that on the body hull, an integral equation can be established for the unknown singularities (sources or mixed sources and dipoles) on the wetted surface of the body only. The hydrodynamic properties on the hull and in the fluid field can then be obtained. In the investigation of tank-wall effects, such a Green function is referred to as the *tank Green function* (TGF) as it satisfies the linearized free-surface condition and the non-penetration condition on the tank bottom and the sidewalls. Obviously, the TGF can be formally represented by an infinite series of mirror

*This study was initiated when the author was employed at the Danish Maritime Institute.

images of the Green function in the open-sea. The convergence of such series, however, is known to be extremely slow.

Morse and Feshbach [1, pp. 814–851] have given comprehensive discussions on different representations of Green functions that describe wave propagation between two parallel planes. These include the method of images, the method of eigenfunctions and the near-field and far-field expansions. In the asymptotic procedure for the method of images described in Morse and Feshbach [1, pp. 815–816], the leading-order influence of the truncated infinite number of images located *far* from the observation point was simply approximated by the Fresnel integrals. Unfortunately, this did not capture the main feature of wave resonance due to the boundary reflections. Recently, the slowly convergent propagating-wave series of mirror images was analyzed by Chen [2] in the evaluation of the Green function of free-surface wave problems in a channel. The study showed that the influence of the infinite number of images located *far* from the observation point may be accurately approximated by means of single integrals. Valuable explicit criteria were obtained in the Green function analysis of Chen [2] for the configuration of a wave tank to avoid reflections of transverse evanescent wave perturbations and for the measurement duration in a wave tank to limit the influence of the reflected propagating waves.

In order to avoid using image series, Kashiwagi [3] formulated a closed-form TGF for the problem of infinite water depth. Computational results for radiation and diffraction forces acting on an offshore structure were obtained by numerically evaluating a double integral over a semi-infinite domain in the TGF expression. Vazquez and Williams [4, 5] reported numerical calculations for the diffraction and radiation problems of a three- dimensional body in a narrow tank with finite depth by using an eigenfunction expansion of the TGF. For each source-field point combination, the number of terms used in the Green function derivative series was determined adaptively according to specified convergence criteria. More terms are required in the vicinity of a tank resonant frequency, particularly when the field point is close to the source point. Linton [6] published a derivation of TGF expressions by representing the wall effect on a point source in an unbounded fluid as a Fourier series whose coefficients are modified Bessel functions. The Fourier-series coefficients are modified to account for the free-surface and bottom boundary conditions by invoking integral representations for modified Bessel functions. The infinite series contained in such expressions converge much more rapidly than the series that are obtained if a simple set of images is used. However, the individual terms in the series are more complicated and the convergence deteriorates when the field point is close to the source point or both the source and field points approach the free surface. No computational practices have been found in the literature that make use of Linton's [6] TGF expressions. Generally speaking, expansions in eigenfunctions and closed-form representations with double integrals are computationally demanding.

It is noted that, although some researchers have published computational results for fluid forces and wave-induced motions of fixed or floating bodies in a channel based on boundary-element methods and numerical evaluation of the tank Green function, no tabulated or plotted results have been found in the literature for the validation of the Green function itself.

The objective of the present study is to reveal analytically the characteristics of wave resonance in narrow wave tanks and to facilitate the use of the *method of images* in accurate and efficient evaluation of the Green function of channel problems. The complete series of images is divided into three groups: images in a near field, images in a middle field and the rest of the infinite number of images in the complementary far field. The part of the Green function induced by the near field images is evaluated in an exact manner based on

the calculation of the open sea Green function. The part induced by the middle field images is estimated by evaluating in an exact form the propagating waves, ignoring the evanescent wave effect. Finally, the part of the Green function induced by the far-field images is asymptotically expressed by a plane-wave approximation plus a parabolic correction, which have equivalent single integral forms instead of the slowly convergent series representation. The evaluation of the influence of the infinite number of images located *far* from the observation point can then be accurate and efficient. It is found from the asymptotic analysis of the far field influence that the tank Green function has a one-sided square-root singularity respectively for the real and the imaginary part, when the excited wave frequency approaches a resonant wave frequency.

Along with the theoretical development in Sections 2 and 3 of this paper, convergence criteria are derived in Section 4 for the different parts of the tank Green function. In Section 5, numerical techniques are described, particularly the asymptotic solution of the part of the tank Green function induced by the far field images. Section 5 also gives the some numerical results of the Green function using the present expressions. As no published results for TGF have been found for comparison, a test procedure is described to demonstrate that the present tank Green function solution has an absolute accuracy of 10^{-5}. The Green function solution is applied to the wave-interference problem of a cylinder in a channel and verified with the published semi-analytical solution.

The present study also has relevance in the mathematical modeling of the field problems between parallel planes that arise in other physics such as acoustics, electrostatics and electromagnetics.

2. Formulation of the Green function

The Cartesian coordinate system o-xyz is defined as an 'equilibrium' set of axes with ox along the longitudinal direction of the wave tank. The $z = 0$ plane corresponds to the calm water level, and z is positive upwards. The x-z plane is coincident with the center- plane of the tank. We assume an ideal fluid and irrotational flow, ω is the oscillating frequency of the fluid motion and the time dependence is of the form $\mathrm{e}^{-\mathrm{i}\omega t}$. The tank Green function is denoted by $G(x, x')$ which represents the spatial part of the velocity potential at a field point $x = (x, y, z)$ in the wave tank due to a pulsating source of unit strength at the point$x' = (x', y', z')$. The TGF must satisfy the following governing equations

$$\begin{cases} \nabla^2 G(x, x') = -4\pi\delta(x - x') & \text{in the fluid ,} \\ -\dfrac{\omega^2}{g}G + \dfrac{\partial G}{\partial z} = 0 & \text{on } z = 0 , \\ \dfrac{\partial G}{\partial z} = 0 & \text{on } z = -h , \\ \dfrac{\partial G}{\partial y} = 0 & \text{on } y = \pm\dfrac{b}{2} , \end{cases} \tag{1}$$

where δ is the Dirac delta function, g the gravitational acceleration; h denotes the water depth, b the width of the wave tank. In addition, the Green function must satisfy a radiation condition that states that, at infinity, G is associated only with waves that propagate away from the source.

The solution of (1) can be obtained by considering an infinite number of images of the source at the positions $x'_m = (x', y'_m, z')$ ($m = 0$ represents the source itself), that is

$$G(x, x') = \sum_{m=-\infty}^{\infty} G_m^O \,, \tag{2}$$

where $G_m^O = G^O(x, x'_m)$ is the open-sea Green function satisfying the first three equations in (1), which represents the potential at the field point x due to the m-th image of the source at the point x'_m with the y-coordinate y'_m expressed as

$$y'_m = (-1)^m y' + mb \,. \tag{3}$$

As G_m^O is an axisymmetric function about the vertical axis through the source or image point x'_m, the Neumann boundary condition on the sidewalls in (1) can be verified by differentiating (2) and rewriting the summation for $y = b/2$,

$$\frac{\partial G}{\partial y} = \sum_{m=0}^{\infty} \frac{\partial}{\partial y}(G_{-m}^O + G_{m+1}^O = 0 \tag{4}$$

and for $y = -b/2$,

$$\frac{\partial G}{\partial y} = \sum_{m=0}^{\infty} \frac{\partial}{\partial y}(G_{-m-1}^O + G_m^O) = 0 \,. \tag{5}$$

The open-sea Green function G_m^O is given by Wehausen and Laitone [7] in the form of principal-value integral as

$$G_m^O = \frac{1}{r_m} + \frac{1}{r'_m} + P \int_0^{\infty} F(\mu) J_0(\mu \rho_m) \mathrm{d}\mu + \mathrm{i}\Lambda J_0(k_0 \rho_m) \,, \tag{6}$$

where J_0 is the first kind of Bessel function, k_0 satisfies the dispersion relation

$$K_0 \tanh(k_0 h) = \omega^2 / g \tag{7}$$

and where other quantities and functions are defined as

$$\rho_m = \sqrt{(x - x')^2 + (y - y'_m)^2} \,, \tag{8}$$

$$r_m = \sqrt{\rho_m^2 + (z - z')^2} \,, \tag{9}$$

$$r'_m = \sqrt{\rho_m^2 + (z + z' + 2h)^2} \,, \tag{10}$$

$$F(\mu) = \frac{(\mu + \nu)\mathrm{e}^{-2\mu h} \cosh \mu(z + h) \cosh \mu(z' + h)}{(\mu - \nu) - (\mu + \nu)\mathrm{e}^{-2\mu h}} \,, \tag{11}$$

$$\Lambda = \frac{2\pi (k_0^2 - \nu^2) \cosh k_0(z + h) \cosh k_0(z' + h)}{(k_0^2 - \nu^2)h + \nu} \tag{12}$$

with

$$\nu = \omega^2/g \ . \tag{13}$$

The integral form (6) is computationally inefficient. This is mainly due to the singularity and oscillations in the integrand, which makes it necessary to employ quite a large number of points in the quadrature used in the estimation of the integral. Therefore, careful treatment is needed (*e.g.* Newman [8]). Alternatively, a series expansion of (6) presented by John [9], which has been proven very efficient when ρ_m is not small, can be written as

$$G_m^O = \zeta_0(z, z')H_0(k_0\rho_m) + \sum_{n=1}^{\infty} \zeta_n(z, z')K_0(k_n, \rho_m) \ , \tag{14}$$

where the first term represents the propagating wave and the summation describes the evanescent wave effect; H_0 and K_0 are, respectively, the Hankel function of the first kind and the modified Bessel function; k_n are defined as the evanescent wave number, which are real positive solutions of the equation

$$k_n \tan(k_n h) = -\omega^2/g \ . \tag{15}$$

The z-dependent functions in (14) are defined as

$$\zeta_0(z, z') = \mathrm{i}\Lambda \ , \tag{16}$$

$$\zeta_n(z, z') = \frac{8k_n}{2k_n h + \sin(2k_n h)} \cosh k_n(z + h) \cos k_n(z' + h) \ . \tag{17}$$

The slowly convergent image series (2) can be rewritten as a sum of three parts,

$$G = G^N + G^M + G^F \tag{18}$$

with G^N the potential induced by a finite series of source and images in a near field,

$$G^N = \sum_{m=-M_0}^{M_0} G_m^O \tag{19}$$

and G^M the potential induced by a finite series of images in a middle field, where the evanescent wave effect can be neglected,

$$G^M = \zeta_0(z, z') \sum_{m=M_0+1}^{2M_1-1} \left[H_0(k_0\rho_m) + H_0(k_0\rho_{-m})\right] \ . \tag{20}$$

In Equation (18), G^F represents the potential induced by the remaining infinite number of images in the far field, which can be expressed only by propagating waves as

$$G^F(\zeta_0(z, z') \sum_{l=1}^{4} \sum_{m=0}^{\infty} H_0(R_{ml}) \ , \tag{21}$$

where R_{ml} denotes the non-dimensional horizontal distance between the field point and the source (or image) point defined by

$$R_{ml} = \sqrt{X^2 + Y_{ml}^2} \quad m = 0, 1, 2, 3, 4 \tag{22}$$

with

$$X = k_0(x - x') \,, \quad Y_{ml} = 2k_0 b(m + Y_m) \,, \tag{23}$$

where $Y_l (l = 1, 2, 3, 4)$ are the non-dimensional transverse distances between the field point and the nearest four images in the far field,

$$\begin{aligned} Y_1 &= M_1 - (y - y')/(2b), \;\; Y_3 = M_1 + 1/2 - (y + y')/(2b) \,, \\ Y_2 &= M_1 + (y - y')/(2b), \;\; Y_4 = M_1 + 1/2 + (y + y')/(2b) \,. \end{aligned} \tag{24}$$

Despite the z-dependence, evaluation of Equation (21) is relevant to a number of wave-propagation problems between parallel walls in other areas of physics, such as acoustics [1].

The derivatives of the TGF are necessary in the boundary-element method. They can be found by differentiation of (18), and are summarized in the Appendix.

With the techniques developed by, for example, Newman [8, 10] and Teste and Noblesse [11], the evaluation of the integral form (6) of the open-sea Green function can be very fast. This, combined with the faster John series (14), provides efficient algorithms for the calculation of G^N and the derivatives. The calculation of G^M and its derivatives is based on the evaluation for the Hankel functions of zero and first order. It is efficient provided that the truncation number M_1 is not very large. It will be shown that, if all the images in (21) are located *far enough* from the tank, the potential G^F and its derivatives have simple and accurate asymptotic expressions in the *vicinity of the source*, whose numerical evaluation is easy and rapid.

3. Asymptotic analysis for G^F

The Hankel function in (21) can be expanded by use of Graf's addition theorem [12, (9.1.79), p. 363],

$$H_0(R_{ml} = \sum_{n=0}^{\infty} \alpha_n (-1)^n J_{2n}(X) H_{2n}(Y_{ml}) \,, \tag{25}$$

where $\alpha_0 = 1$ and $\alpha_n = 2$ when $n \geq 1$; $J_{2n}(X)$ and $H_{2n}(Y_{ml})$ are the first-kind Bessel and Hankel functions of $2n$-th order. The expansion (25) is absolutely convergent when $|X| < |Y_{ml}|$.

When Y_{ml} is large, the Hankel function in (25) can be asymptotically expressed [12, Equation (9.2.7), p. 364] as

$$H_{2n}(Y_{ml}) = (-1)^n c \mathrm{e}^{\mathrm{i}Y_{ml}} (Y_{ml}^{-1/2} + \mathrm{i}c_n Y_{ml}^{-3/2} + \Re_{mn}) \,, \tag{26}$$

where the constants are given by $c = \mathrm{e}^{-\mathrm{i}\pi/4}\sqrt{2/\pi}$ and $c_n = (16n^2 - 1)/8$, and the error term $\Re_{mn}$ is governed by the first neglected term of the asymptotic series [13] as

$$|\Re_{mn}| < \frac{(16n^2 - 1)(16n^2 - 9)}{128} Y_{ml}^{-5/2} \,. \tag{27}$$

Invoking the asymptotic expression (26) for the Hankel function, substitution of (25) in (21) we have

$$G^F = c\zeta_0(z, z')) \sum_{l=1}^{4} \left[\eta_1(Y_l) + \xi_2(X)\eta_2(Y_l) + \Re \right] \,, \tag{28}$$

where

$$\xi_2(X) = \frac{1}{2}X^2 - \frac{1}{8}\,, \tag{29}$$

$$\eta_1(Y_l) = \frac{\mathrm{e}^{2\mathrm{i}BY_l}}{\sqrt{2\pi B}} \int_0^\infty \frac{t^{-1/2}\mathrm{e}^{-Y_l t}}{1-\mathrm{e}^{-t+\mathrm{i}2B}}\,\mathrm{d}t\,, \tag{30}$$

$$\eta_2(Y_l) = \frac{\mathrm{i}\mathrm{e}^{2\mathrm{i}BY_l}}{\sqrt{2\pi B}B} \int_0^\infty \frac{t^{1/2}\mathrm{e}^{-Y_l t}}{1-\mathrm{e}^{-t+\mathrm{i}2B}}\,\mathrm{d}t\,, \tag{31}$$

with $B = k_0 b$ the non-dimensional tank width.

Based on (27), the error term in (28) is bounded by

$$|\Re| < |\xi_3(X)\eta_3(Y_l)|\,, \tag{32}$$

where

$$\xi_3(X) = \frac{1}{128}(16X^4 + 24X^2 + 9) \tag{33}$$

and

$$\eta_3(Y_l) = \frac{\mathrm{e}^{2\mathrm{i}BY_l}}{3\sqrt{2\pi B}B^2} \int_0^\infty \frac{t^{3/2}\mathrm{e}^{-Y_l t}}{1-\mathrm{e}^{-t+\mathrm{i}2b}}\,\mathrm{d}t\,. \tag{34}$$

The following identities have been used in the derivation of (28) and (32),

$$\sum_{n=0}^{\infty} \alpha_n J_{2n}(X) = 1\,, \tag{35a}$$

$$\sum_{n=0}^{\infty} c_n \alpha_n J_{2n}(X) = \frac{1}{2}X^2 - \frac{1}{8}\,, \tag{35b}$$

$$\sum_{n=0}^{\infty} \alpha_n (16n^2-1)(16n^2-9) J_{2n}(X) = (16X^4 + 24X^2 + 9) \tag{35c}$$

and

$$\sum_{m=0}^{\infty} \frac{\mathrm{e}^{2\mathrm{i}Bm}}{\sqrt{(m+Y_l)}} = \frac{1}{\sqrt{\pi}} \int_0^\infty \frac{t^{-1/2}\mathrm{e}^{-Y_l t}}{1-\mathrm{e}^{-t+\mathrm{i}2B}}\mathrm{d}t, \tag{36a}$$

$$\sum_{m=0}^{\infty} \frac{\mathrm{e}^{2\mathrm{i}Bm}}{\sqrt{(m+Y_l)^{3/2}}} = \frac{2}{\sqrt{\pi}} \int_0^\infty \frac{t^{1/2}\mathrm{e}^{-Y_l t}}{1-\mathrm{e}^{-t+\mathrm{i}2B}}\mathrm{d}t, \tag{36b}$$

$$\sum_{m=0}^{\infty} \frac{\mathrm{e}^{2\mathrm{i}Bm}}{\sqrt{(m+Y_l)^{5/2}}} = \frac{4}{3\sqrt{\pi}} \int_0^\infty \frac{t^{3/2}\mathrm{e}^{-Y_l t}}{1-\mathrm{e}^{-t+\mathrm{i}2B}}\mathrm{d}t. \tag{36c}$$

The identity (35a) can be found in [12, (9.1.46), p. 361], while we may verify (35b) and (35c) by repeatedly using (9.1.41) and its differentiation, also in [12, p. 361]. Equation (36) can be deduced from Lipschitz's formula [14, p. 28]. Equations (36a) and (36b) have been used by Chen [2] in the Green function analysis, while transforms similar to (36a) have been used by Eatock Taylor and Hung [15] and Yeung and Sphaier [16] in the semi-analytical solutions for a vertical cylinder in a wave tank to account for the influence of the complete infinite number of image cylinders.

The derivatives of the far-field part of the Green function are obtained by differentiating the asymptotic expression (28) and are presented in the Appendix.

It is seen that the summation over the infinite number of images in the far field is now expressed in (28) by Y_l-dependent functions $\eta_1(Y_l)$ and $\eta_2(Y_l)$ which have single integral representations as given by (30) and (31). The single integral representations are much more advantageous than the slowly convergent infinite series due to the fact that the kernels are smooth functions with an exponentially decaying component; the numerical evaluation is then easy and rapidly convergent. Physically, the first term in the brackets in the asymptotic expression (28) represents a plane-wave approximation, whereas the second term gives a correction. The plane-wave term exhibits a very important feature of the tank wall effects, that is, tank resonance occurs when the tank width is an integer multiple of half the wavelength, where both the infinite series and the integral expression of $\eta_1(Y_l)$ have singularities. No matter how large the truncation number M_1 is, the singularity exists in the far-field solution. Therefore, the tank resonance cannot be properly modeled by taking only a finite number of images in the Green-function calculation.

It is important to know the singular behavior of the tank resonance when the excited wave number approaches a resonant wave number, *i.e.* when $B \to n\pi, n = 0, 1, 2, 3, \ldots$.

In this case the main contribution to the integral of $\eta_1(Y_l)$ is near the singular point $t = 0$. Therefore, by denoting that $\varepsilon = 2|B - n\pi|$, we have

$$\eta_1(Y_l) = \frac{\mathrm{e}^{2\mathrm{i}BY_l}}{\sqrt{2\pi B}} \int_0^\infty \frac{t^{-1/2}\mathrm{e}^{-Y_l t}}{1 - \mathrm{e}^{-t+\mathrm{i}2B}}\mathrm{d}t = \frac{\mathrm{e}^{2\mathrm{i}BY_l}}{\sqrt{2\pi B}} \int_0^1 \frac{t^{-1/2}\mathrm{e}^{-Y_l t}}{1 - \mathrm{e}^{-t+\mathrm{i}\varepsilon\,\mathrm{sign}(B-n\pi)}}\mathrm{d}t + O(1), \quad \text{when } \varepsilon \to 0\,, \tag{37}$$

where $\mathrm{sign}(B - n\pi)$ is the sign of $(B - n\pi)$. Taylor's expansion of $\mathrm{e}^{-t+\mathrm{i}\varepsilon\mathrm{sign}(B-n\pi)}$ shows that

$$\begin{aligned} \int_0^1 \frac{t^{-1/2}}{1 - \mathrm{e}^{-t+\mathrm{i}\varepsilon\mathrm{sign}(B-n\pi)}}\mathrm{d}t &= \int_0^1 \frac{t^{-1/2}}{t - \mathrm{i}\varepsilon\mathrm{sign}(B - n\pi)}\mathrm{d}t + O(1) \\ &= \frac{2}{\sqrt{\varepsilon}} \int_0^{1/\sqrt{\varepsilon}} \frac{u^2 + \mathrm{i}\ \mathrm{sign}(B - n\pi)}{1 + u^4}\mathrm{d}u + O(1)\,. \end{aligned} \tag{38}$$

The last integral can be approximated by

$$\int_0^\infty \frac{u^2 + \mathrm{i}\ \mathrm{sign}(B - n\pi)}{1 + u^4}\mathrm{d}t = \frac{\pi[1 + \mathrm{i}\ \mathrm{sign}(B - n\pi)]}{2\sqrt{2}}$$

with an error of $O(\sqrt{\varepsilon}$. Thus, the asymptotic behavior of $\eta_1(Y_l)$ can be expressed as

$$\eta_1 = \sqrt{\frac{\pi}{2B\varepsilon}}\mathrm{e}^{\mathrm{i}2n\pi Y_l}\mathrm{e}^{\mathrm{i}\frac{\pi}{4}\mathrm{sign}(B-n\pi)} + O(1), \quad \text{when } \varepsilon \to 0\,. \tag{39}$$

Substitution of (39) in (28) gives

$$G^F = \frac{2}{\sqrt{B\varepsilon}}\Lambda(z,z')\left\{\cos\left[n\pi(y-y')/b\right] + (-1)^n\cos\left[n\pi(y+y')/b\right]\right\}\times \\ \mathrm{e}^{\mathrm{i}\frac{\pi}{4}[1+\mathrm{sign}(B-n\pi)]} + O(1), \quad \text{when } \varepsilon \to 0\ . \tag{40}$$

This indicates that the real part of G^F has a one-sided square-root singularity when $B \to n\pi$ from the smaller side, while the imaginary part of G^F has the singularity when $B \to n\pi$ from the greater side.

The asymptotic expression (40) is independent of Y_l and, therefore, may be extended for the infinite propagating-wave series, which includes all the mirror images. As the evanescent-wave modes do not exhibit wave resonance, it is expected that the tank Green function G contains the same singularity as in G^F. The detailed asymptotic analysis for the resonant behavior in G may be quite lengthy. A square-root singularity has been reported by Yeung and Sphaier [16] for the added mass and damping coefficients of a truncated cylinder in a channel.

4. Convergence criteria

In this section we discuss the convergence criteria for the evaluation of the potentials induced by the images in the middle and far fields, and give some simple expressions for the determination of the truncation numbers M_0 and M_1.

In order to simplify the analysis of the part of the Green function induced by the middle and far-field images, the evanescent-wave effect in the open-sea Green function (14) has been ignored in the approximations (20) and (21). The error can be found by means of the asymptotic expression of the modified Bessel function $K_0(k_n\rho_m)$ for large arguments. In this case the evanescent-wave series is dominated by the first term where $K_0(k_1\rho_m)$ can be expressed asymptotically as

$$K_0(k_1\rho_m) \approx \sqrt{\frac{\pi}{2k_1\rho_m}}\mathrm{e}^{-k_1\rho_m}\ . \tag{41}$$

As the evanescent-wave number k_1 satisfies the relation $k_1\tan(k_1h) = -\omega^2/g$, we have

$$\frac{\pi}{2} < k_1h < \pi\ . \tag{42}$$

By using (3) and the truncation notation in (19), we have that the distance between any field points in the tank and the images in the middle or far field satisfies

$$\rho_m \geq (|m|-1)b \geq M_0b\ . \tag{43}$$

Substitution of (41) and (42) in (40), therefore, provides that

$$K_0(k_1\rho_m)\sqrt{\frac{h}{M_0b}}\mathrm{e}^{-\frac{\pi bM_0}{2h}}\ . \tag{44}$$

This equation gives a criterion for the truncation number M_0. For example, if at least five-figure precision is required, the truncation number is approximately bounded by

$$M_0 \geq 1 + \mathrm{Int}(7h/b) \ . \tag{45}$$

We obtain Equation (45) by assuming $h/b = O(1)$. If $h \to \infty$, we have $\zeta_n(z, z') \to O(h^{-1})$, based on (17) and (42). This, combined with (44), may provide another criterion for the truncation number M_0 for deep-water cases.

The truncation number M_1 determines the distance between the field point and the nearest images in the far field, Y_l, and hence the convergence and accuracy of the asymptotic solution. First of all, the convergence of the series expansion (25) requires that

$$M_1 > |X| + (2b)^{-1}|y - y'| \ . \tag{46}$$

The truncation number M_1 is also essential for the numerical precision of the asymptotic expression (28), where the propagating waves of the far field images are expressed by the plane-wave approximation plus a correction. The error function is defined by (32). From Equation (34), we have

$$|\eta_3(Y_l)| < \frac{1}{3\sqrt{2\pi}(BY_l)^{5/2}} \max\{6{\cdot}4, Y_l\} \ . \tag{47}$$

Thus, in order to guarantee an absolute accuracy of 10^{-5} for the approximation of (21) by (28), we may use the following condition

$$\begin{aligned} M_1 > \ & \max\left\{13{\cdot}5B^{-1}(X^4 + 1{\cdot}5X^2 + 0{\cdot}5625)^{-\frac{5}{3}}(X^4 + 1{\cdot}5X^2 + 0{\cdot}5625)^{\frac{2}{3}}\right\} \\ & + (2b)^{-1}|y - y'| \ . \end{aligned} \tag{48}$$

Because the negligence of the evanescent-wave effect is necessary for the far-field approximation, another restriction has to be set for the truncation number M_1,

$$M_1 \geq (M_0 + 1)/2 \ . \tag{49}$$

In the case of using the equality in (49), M_0 has to be taken as an odd number so that all the images can be included in either near or far field.

It is seen from (46) and (48) that the present analysis for the TGF is more efficient for small $|X|$ due to the fact that high accuracy can be reached when a small number of images is used in the middle field. In other words, the plane-wave approximation plus the parabolic correction for the far-field images is more effective when the observation point is close to the vertical plane through the source and images. Conditions (45), (46), (48) and (49) all have to be satisfied in the numerical solution of the tank Green function presented in this paper.

5. Numerical solution

As mentioned in the end of Section 2, much effort has been made to calculate efficiently the open-sea Green function by, for example, Newman [8, 10] and Teste and Noblesse [11]. These form a good basis for the evaluation of the tank Green function formulated in the present paper, but they are not repeated here. The numerical solution in this paper for the open-sea Green function has been verified by Pidcock [17] results with very good agreement.

The evaluation for G^F is based on the numerical integration of the single integrals defined in (30) and (31). As the integrands are smooth functions with exponentially decreasing component, accurate and efficient numerical integration can be achieved by integration rules of

Table 1. Tank Green Function and the xyz-derivatives for $k_0b = 3{\cdot}1$; $h/b = 0{\cdot}5$, $(x, y, z) = (0{\cdot}2b, 0{\cdot}01b, 0{\cdot}0)$, $(x', y', z') = (0{\cdot}0, 0{\cdot}1b, 0{\cdot}0)$.

	Real part		Imaginary part	
	M_0=9 M_1=18	M_0=9 M_1=30	M_0=9 M_1=18	M_0=9 M_1=30
$G^F h$	3·509596E-01	−2·643842E-01	−6·144126E-01	−4·722516E-01
$G^M h$	1·000805E+00	1·616141E+00	7·986270E-01	6·564695E-01
$G^N h$	−6·178405E-01	−6·178405E-01	4·188264E+00	4·188264E+00
Gh	7·339239E-01	7·339165E-01	4·372478E+00	4·372482E+00
$G_x^F h^2$	5·111367E-03	2·710823E-03	3·880662E-03	−1·187938E-03
$G_x^M h^2$	−1·880335E-02	−1·642792E-02	3·730163E-02	4·238579E-02
$G_x^N h^2$	−1·797648E+01	−1·797648E+01	−4·879619E+00	−4·879619E+00
$G_x h^2$	−1·799017E+01	−1·799020E+01	−4·838436E+00	−4·838421E+00
$G_y^F h^2$	−5·702604E+00	−1·045881E+01	−1·148211E+01	−4·655023E-01
$G_y^M h^2$	1·939781E+01	2·415393E+01	−1·475350E+00	−1·249182E+01
$G_y^N h^2$	2·069194E+01	2·069194E+01	1·295730E+01	1·295730E+01
$G_y h^2$	3·438715E+01	3·438707E+01	−1·535416E-04	−2·288818E-05
$G_z^F h^2$	4·970878E-01	−3·744652E-01	−8·702340E-01	−6·688818E-01
$G_z^M h^2$	1·417507E+00	2·289050E+00	1·131149E+00	9·298021E-01
$G_z^N h^2$	−8·750901E-01	−8·750901E-01	5·932120E+00	5·932120E+00
$G_z h^2$	1·039505E+00	1·039495E+00	6·193036E+00	6·193041E+00

Gauss type. First, the semi-infinite interval is cut into a finite domain [0, 1] and the remaining semi-infinite domain $[1, \infty]$. The 15-point Gauss-Laguerre rule is used directly for the infinite-domain integration. The non-uniform coordinate stretchings $t_1 = \sqrt[4]{t}$ and $t_2 = \sqrt{t}$ are performed, respectively, for the finite-domain integration in $\eta_1(Y_l)$ and $\eta_2(Y_l)$ in order to remove the singularity at the origin and to further smooth the integrands, particularly in the vicinity of resonant frequencies. The 40- point Gauss-Legendre rule is then employed for the finite-domain integration in the strained coordinates. At least five-figure precision can be reached in the numerical evaluation of $\eta_1(Y_l)$ and $\eta_2(Y_l)$.

Some numerical examples show that the computational time for the TGF by the present procedure is several times that for the open-sea Green function. The computational time for G^F is only a small part of the total time of the tank Green function calculation.

In order to demonstrate the accuracy of the present TGF solutions, Table 1 compares some numerical results calculated under the same input conditions, $k_0b = 3{\cdot}1$, $h/b = 0{\cdot}5$, $(x, y, z) = (0{\cdot}2b, 0{\cdot}0)$ and $(x', y', z') = (0{\cdot}0, 0{\cdot}1b, 0{\cdot}0)$, but with different image arrangements in the middle and far field. It is shown in Table 1 that by increasing the number of images in the middle field, numerical results for the tank Green function and the xyz-derivatives change within an absolute error of 10^{-5}, although both the middle-field solution and the far-field solution vary significantly. The influence of the far-field images does not seem to reduce for the given wave number when the number of images in the middle field increases from 52 to 100 (corresponding, respectively, to $M_1 = 18$ and 30). The accuracy of the TGF and its derivatives has also been tested for different source- field point combinations and different

1

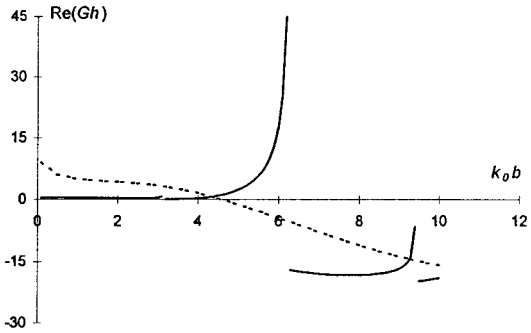

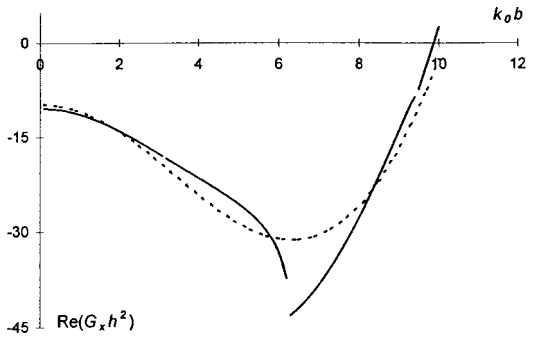

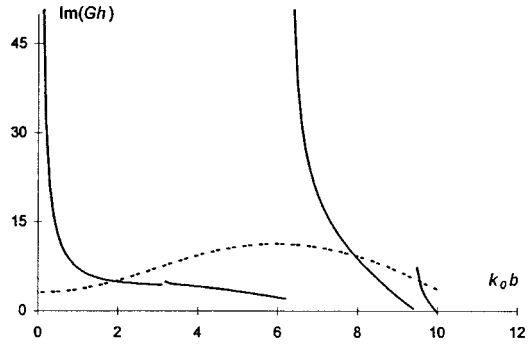

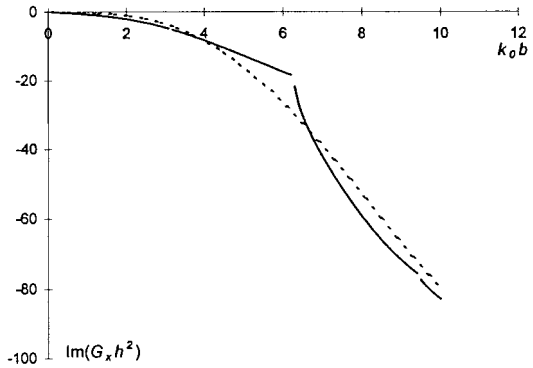

Figure 1. Real part (up) and imaginary part (down) of the tank Green function *vs.* the wave number. Dashed lines are solutions of the open-sea Green function. $(x, y, z) = (0{\cdot}2b, 0{\cdot}01b, 0{\cdot}0)$; $(x', y', z') = (0{\cdot}0, 0{\cdot}01b, 0{\cdot}0)$; $h/b = 0{\cdot}5$.

Figure 2. Real part (up) and imaginary part (down) of the x-derivative of the tank Green function *vs.* the wave number. Dashed lines are solutions of the open-sea Green function. $(x, y, z) = (0{\cdot}2b, 0{\cdot}01b, 0{\cdot}0)$; $(x', y', z') = (0{\cdot}0, 0{\cdot}01b, 0{\cdot}0)$; $h/b = 0{\cdot}5$.

wave numbers by increasing the number of images in the near field or both image numbers in the near and middle field. Good consistency has been obtained.

Figure 1–4 illustrate the non-dimensional tank Green function and its derivatives as functions of the non-dimensional wave number. The tank configuration and the source and observation-point positions are the same as for Table 1. It is seen from these figures that the tank Green function is very different from the open-sea Green function, particularly in the vicinity of the resonant points $k_0b = 0, \pi, 2\pi, 3\pi, \ldots$. These resonant regions characterize the tank-wall effects and should be treated carefully in the experimental and computational analyses of hydrodynamic wave problems in a channel. The square-root singular behavior as indicated in (40) is demonstrated in the numerical solution, except for G_x, as no resonances occur in the longitudinal mode. In fact, if more computational points are added to Figure 2 to approach the resonant frequencies, it will be seen that G_x is continuous.

The numerical solution of the tank Green function presented above is implemented in a three-dimensional boundary-element-method software package to predict wave- body interactions in a channel. To validate its effectiveness, it is applied to investigate the wave-

1

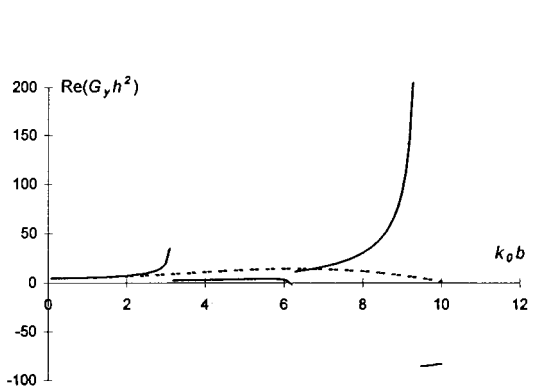

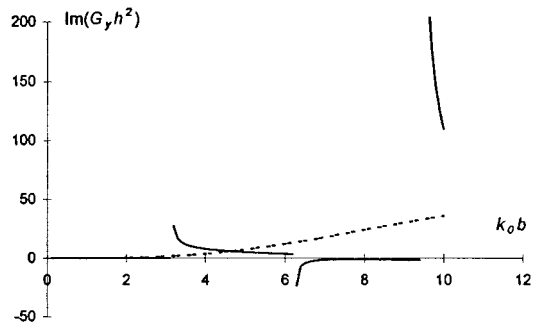

Figure 3. Real part (up) and imaginary part (down) of the y-derivative of the tank Green function *vs.* the wave number. Dashed lines are solutions of the open-sea Green function.$(x, y, z) = (0{\cdot}2b, 0{\cdot}01b, 0{\cdot}0)$; $(x', y', z') = (0{\cdot}0, 0{\cdot}01b, 0{\cdot}0)$; $h/b = 0{\cdot}5$.

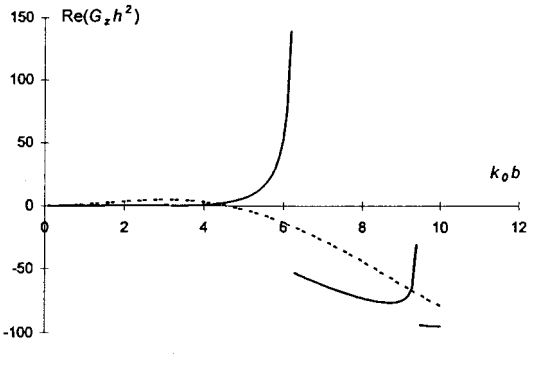

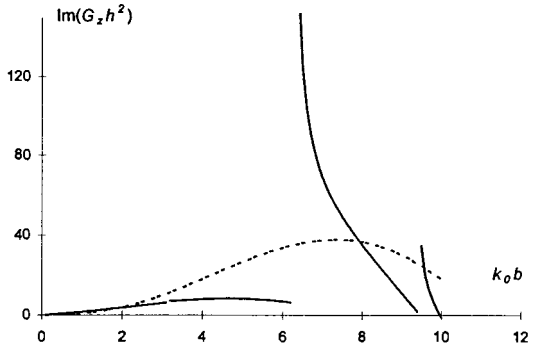

Figure 4. Real part (up) and imaginary part (down) of the z-derivative of the tank Green function *vs.* the wave number. Dashed lines are solutions of the open-sea Green function. $(x, y, z) = (0{\cdot}2b, 0{\cdot}01b, 0{\cdot}0)$; $(x', y', z') = (0{\cdot}0, 0{\cdot}01b, 0{\cdot}0)$; $h/b = 0{\cdot}5$.

interference effects on a truncated cylinder in a channel, which have been studied semi-analytically by Yeung and Sphaier [16]. In the present numerical investigation, the surface of the cylinder is panelized as 448 facets with 6 equally divided intervals in depth, 4 in radial direction and 32 in circumference. The top of the cylinder is also panelized as a mathematical lid to suppress a possible appearance of irregular frequencies. The cylinder is placed in the center of the channel. The computation is performed on a HP workstation.

Figure 5 demonstrates the non-dimensional added-mass and damping coefficients for heave motion as a function of $k_b/(2\pi)$. We obtained good agreement is obtained between the semi-analytical solution [16] and the numerical computation using the present Green-function evaluation and only 448 body-surface panels, showing the robustness of the new algorithm. It is noted that the plot of the present numerical results is based on a more sparse set of data with a straight-line fit between adjacent points.

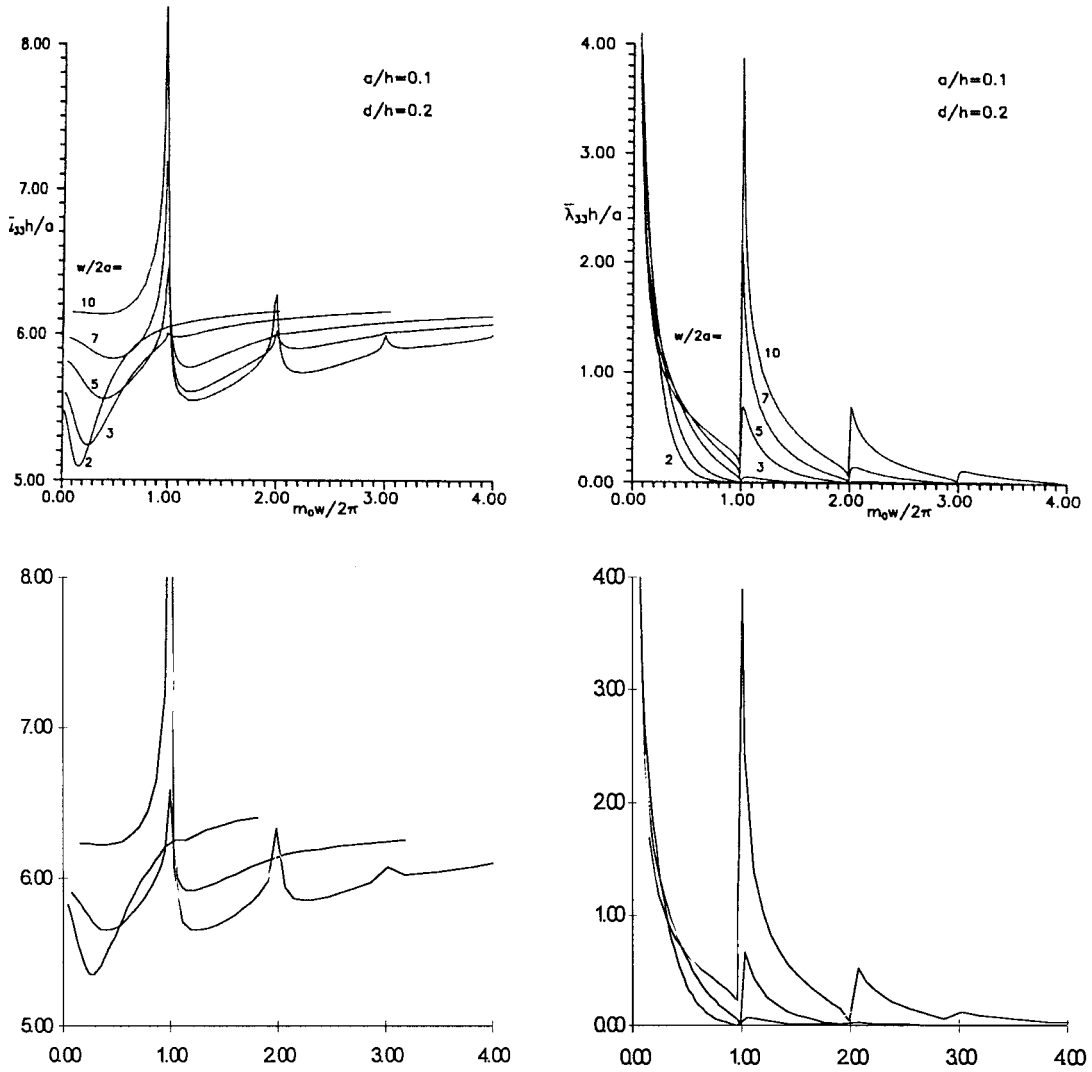

Figure 5 Non-dimensional added mass (left) and damping (right) coefficients for heave motion of a cylinder in a channel. Above is the semi-analytical solution of Yeung and Sphaier [16], where a and d denote the cylinder radius and draft; w, the channel width; $m_0 w = k_0 b$ according to the present notation. Below is the present numerical solution for $b/2a = 3, 5, 7, 10$.

6. Concluding remarks

A consistent asymptotic analysis has been presented in this paper for the Green function in hydrodynamic-wave problems in a channel to account for the influence of the infinite number of wall images. It is clear from this analysis that channel-wall effects are difficult to model when only a finite number of images are used. However, based on the asymptotic analysis, the influence of the infinite number of images can be accurately and efficiently taken into account by the plane-wave approximation plus the parabolic correction. This procedure is valid for all source-field point combinations, but the numerical efficiency increases when the distance along the channel between the source and the field point decreases. Also, based on the asymptotic analysis, it has been shown that the Green function has a square-root singular

behavior due to the sidewalls at the frequencies corresponding to the occurrence of transverse resonant modes in the channel. Numerical results have verified the theoretical expressions and the robustness of the algorithm. Based on the asymptotic analysis of channel resonance, rapidly convergent series expressions for (30) and (31) may be developed to further accelerate the numerical algorithm.

Acknowledgements

This study was financially supported in part by the Danish Maritime Institute and the Danish Academy of Technical Sciences and in part by the Australian Research Council Small Grant scheme. The author wishes to thank Dr. John Christoffersen of the Danish Maritime Institute, Professor Yishan Dai of Harbin Engineering University and Professor Beverley Ronalds of The University of Western Australia for valuable discussions. Reviewers' comments are acknowledged.

Appendix: Derivatives of the tank Green function

The derivatives of the TGF are necessary in the boundary-element method. They can be found by differentiating (18),

$$\left(\frac{\partial}{\partial x}, \frac{\partial}{\partial y}, \frac{\partial}{\partial z}\right) G = \left(\frac{\partial}{\partial x}, \frac{\partial}{\partial y}, \frac{\partial}{\partial z}\right) \left(G^N + G^M + G^F\right) . \tag{A1}$$

The derivatives of the near-field part of the Green function can be expressed in terms of the open-sea Green function as

$$\begin{aligned} &\frac{\partial}{\partial x} G^N = \sum_{m=-M_0}^{M_0} \frac{x - x'}{\rho_m} \frac{\partial}{\partial \rho_m} G_m^O , \quad \frac{\partial}{\partial y} G^N = \sum_{m=-M_0}^{M_0} \frac{y - y'_m}{\rho_m} \frac{\partial}{\partial \rho_m} G_m^O , \\ &\frac{\partial}{\partial z} G^N = \sum_{m=-M_0}^{M_0} \frac{\partial}{\partial z} G_m^O . \end{aligned} \tag{A2}$$

The derivatives of the middle-field part of the Green function can be represented by the Hankel functions as

$$\begin{aligned} \frac{\partial}{\partial x} G^M &= -k_0 \zeta_0(z, z')(x - x') \sum_{m=M_0+1}^{2M1-1} \left[\frac{H_1(k_0 \rho_m)}{\rho_m} + \frac{H_1(k_0 \rho_{-m})}{\rho_{-m}} \right] , \\ \frac{\partial}{\partial y} G^M &= -k_0 \zeta_0(z, z') \sum_{m=M_0+1}^{2M_1-1} \left[\frac{y - y'_m}{\rho_m} H_1(k_0 \rho_m) + \frac{y - y'_{-m}}{\rho_{-m}} H_1(k_0 \rho_{-m}) \right] , \\ \frac{\partial}{\partial z} G^M &= \zeta'_0(z, z') \sum_{m=M_0+1}^{2M_1-1} \left[H_0(k_0 \rho_m) + H_0(k_0 \rho_{-m}) \right] . \end{aligned} \tag{A3}$$

Hereafter $\zeta'_0(z, z')$ denotes the derivative of $\zeta_0(z, z')$ with respect to z.

The derivatives of the far field part of the Green function are obtained by differentiating the asymptotic expression (28) as

$$\begin{aligned}
\frac{\partial}{\partial x}G^F &= ck_0\zeta_0(z,z')X\sum_{l=1}^{4}\eta_2(Y_l)\ ,\\
\frac{\partial}{\partial y}G^F &= \mathrm{i}ck_0\zeta_0(z,z')\sum_{l=1}^{4}(-1)^l\left\{\eta_1(Y_l)+\left[\tfrac{1}{2}+\xi_2(X)\right]\eta_2(Y_l)\right\}\ , \qquad \text{(A4)}\\
\frac{\partial}{\partial z}G^F &= c\zeta_0'(z,z')\sum_{l=1}^{4}\left[\eta_1(Y_l)+\xi_2(X)\eta_2(Y_l)\right]\ .
\end{aligned}$$

A higher-order term proportional to $\eta_3(Y_l)$ is neglected in $\dfrac{\partial}{\partial y}G^F$ in (A4).

References

1. P. M. Morse and H. Feshbach, *Methods of Theoretical Physics* (Part 1). New York: McGraw-Hill (1953) 997 pp.
2. X. B. Chen, On the side wall effects upon bodies of arbitrary geometry in wave tanks. *Appl. Ocean Res.* 16 (1994) 337–345.
3. M. Kashiwagi, Radiation and diffraction forces acting on an offshore-structure model in a towing tank. *Int. J. Offshore Polar Eng.* 1 (1991) 101–107.
4. J. H. Vazquez and A. N. Williams, Hydrodynamic loads on a three-dimensional body in a narrow tank. *J. Offshore Mech. Arctic Eng.* 116 (1994) 117–121.
5. J. H. Vazquez and A. N. Williams, Wave radiation by a three-dimensional body in a narrow tank. *Ocean Eng.* 22 (1995) 799–817.
6. C. M. Linton, On the free-surface GreenÆs function for channel problems. *Appl. Ocean Res.* 15 (1993) 263–267.
7. J. V. Wehausen and E. V. Laitone, Surface waves. In: S. Flugge (ed.), *Handbuch der Physik* 9 (III). Berlin: Springer-Verlag (1960) 446–815.
8. J. N. Newman, Algorithms for the free-surface Green function. *J. Eng. Math.* 19 (1985) 57–67.
9. F. John, On the motion of floating bodies (II. simple harmonic motions). *Comm. Pure Appl. Math.* 3 (1950) 45–101.
10. J. N. Newman, Approximation of free-surface Green function. In: P. A. Martin and G. R. Whickham (eds.), *Wave Asymptotics*. Cambridge University Press (1992) 107–142.
11. J. G. Teste and F. Noblesse, Numerical evaluation of the Green function of water- wave radiation and diffraction. *J. Ship Res.* 30 (1986) 69–84.
12. M. Abramowitz and I. A. Stegun, *Handbook of Mathematical Functions*. New York: Dover (1972) 1046 pp.
13. A. Nayfeh, *Perturbation Methods*. New York: John Wiley and Sons (1973) 425pp.
14. H. Bateman, *Higher Trascendental Functions* (1). New York: McGraw-Hill (1953) 302 pp.
15. R. Eatock Taylor and S. M. Hung, Mean drift forces on an articulated column oscillating in a wave tank. *Appl. Ocean Res.* 7 (1985) 66–78.
16. R. W. Yeung and S. H. Sphaier, Wave-interference effects on a truncated cylinder in a channel. *J. Eng. Math.* 23 (1989) 95–117.
17. M. K. Pidcock, The calculation of Green functions in three-dimensional hydrodynamic gravity problems. *Int. J. Num. Meth. Fluids* 5 (1985) 891–909.